RESEARCH OF COLLISION SPEED DEPENDENCY OF PEDESTRIAN HEAD AND CHEST INJURIES USING HUMAN FE MODEL (THUMS VERSION 4)

Ryosuke Watanabe
Hiroshi Miyazaki
Yuichi Kitagawa
Tsuyoshi Yasuki
Toyota Motor Corporation
Japan
Paper Number 11-0043

ABSTRACT

In this research, the collision speed dependency of pedestrian head and chest injuries was investigated using the human FE model THUMS Version 4, independently developed by Toyota Motor Corporation and Toyota Central R&D Labs, Inc. to predict brain and internal organ injuries. In addition, this research also looked at the relationship between impact speed and fatality risk. The study first verified the biofidelity of the THUMS pedestrian model in terms of body region components, such as the head, chest, and lower extremities, and the whole body. The model closely simulated the impact response of each body region component described in the literature. As for the whole body kinematics, the calculated trajectories of each portion of the body during a collision with a vehicle were a good match with those of post mortem human subjects (PMHS) described in the literature. It was also determined that the model predicted injuries at the locations reported in the PMHS tests.
Using the validated THUMS model, this research then looked at the relationship of head and chest injuries with collision speed. Collisions between a pedestrian and an SUV were analyzed at three collision speeds of 30, 40, and 50 km/h. Head injuries did not occur at a collision speed of 30 km/h, but in collisions at 40 and 50 km/h the results suggested that a serious brain injury, known as diffuse axonal injury (DAI), occurred. Furthermore, in regard to the chest area, injuries did not occur at 30 km/h, but at 40 km/h bone fractures in the ribs occurred, and at 50 km/h, in addition to an increase in the number of bone fractures in the ribs, the results suggested that serious injuries to internal organs, such as damage to the heart, also occurred.
These results correspond with the trends in accident data that indicate that the fatality risk for pedestrians increases when the collision speed is 40 km/h or higher.

INTRODUCTION

According to the statistical research of the Traffic Bureau of the National Police Agency, the number of traffic fatalities in Japan in 2009 was 4,914. Pedestrians accounted for 1,717 of this total which is higher than the number of fatalities among vehicle occupants (1,600 people, Figure 1). Looking at the fatalities based on the region of the body that was injured, head injuries accounted for the largest proportion at approximately 54%, followed by chest injuries at approximately 16% (Figure 2) [1].
Anderson et al. (2005) investigated the relationship between collision speed and fatality risk for pedestrians [2]. When the collision speed exceeds 40 km/h, the pedestrian fatality risk increases (Figure 3), but the reason for this has not been determined.
Experimental studies have been conducted to investigate pedestrian injuries using post mortem human subjects (PMHS) and crash test dummies. Schroeder et al. (2008) [3] and Subit et al. (2008) [4] simulated collisions between compact cars, SUVs, and minivans with pedestrians in PMHS tests to analyze the behavior of a pedestrian body during a collision and what kinds of injuries are suffered as a result.
Kerrigan et al. (2008) conducted a series of PMHS tests to investigate the injuries to a pedestrian's lower extremities when impacted by the front end of a small sedan and a large SUV [5]. Kerrigan et al. (2005) also conducted collision tests between an SUV and both PMHS and test dummies to compare the behavior at the time of a collision [6].
In recent years, FE models have been used to simulate injuries to pedestrians in a collision. Yasuki (2005) [7] and Miyazaki et al. (2009) [8] analyzed the difference in impact response between a pedestrian lower extremity and a Transport Research Laboratory (TRL) lower leg impactor (used in assessment tests) in car impacts through FE simulations. Tamura et al. (2006) simulated the behavior of a pedestrian during a collision using a whole body pedestrian model containing a part simulating a brain, and then discussed the possible mechanism of head injuries [9]. As described above, research into pedestrian-to-vehicle collisions mostly focus on the behavior of the lower extremities and injuries such as ligament ruptures and bone fractures of the lower extremities, or on head injuries. However, few studies have been conducted on chest injuries and especially on internal organ injuries.
This paper analyzes the relationship of pedestrian head and chest injuries with the collision speed in vehicle collisions, and then discusses possible factors that increase the fatality risk at a collision speed of 40 km/h or higher. The research used a full-body FE

model called the Total Human Model for Safety (THUMS) Version 4 which includes both the brain and internal organ parts in detail. First, the biofidelity of the THUMS pedestrian model was verified. Impact tests on body region components and car-to-pedestrian impact tests described in the literature were simulated with the model. Impact responses of the model were compared to those in the tests. Next, the research analyzed the relationship between collision speed and head and chest injuries through pedestrian-to-SUV impact simulations at various collision speeds. The finite element analysis code, LS-DYNA^{TM} V971, was used for the simulations.

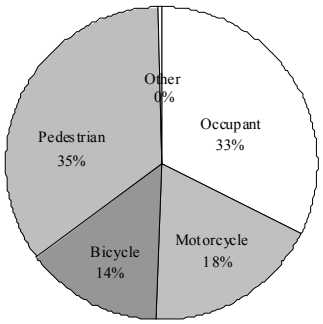

Figure 1. Proportions of traffic accident fatalities according to type.

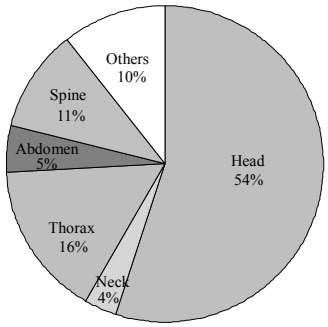

Figure 2. Proportions of injuries suffered by pedestrians in fatal accidents.

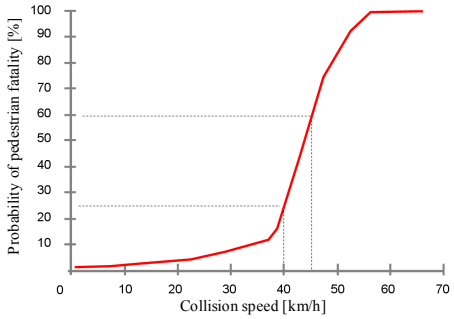

Figure 3. Relationship between collision speed and fatality risk in pedestrian impact.

MODEL VALIDATION

Outline of THUMS Version 4

THUMS is a human body FE model that was jointly developed by Toyota Central R&D Labs, Inc. and Toyota Motor Corporation. Figure 4 shows the physique of the THUMS model in a standing posture. This model simulates a 50th percentile American male with a height of 175 cm and a weight of 77 kg. THUMS Version 4 includes the internal organs of the body, the brain, and the skeleton, in great detail. The number of nodes in the model is approximately 650,000 and the number of elements is approximately 2 million [10]. The geometrical data of the internal organs was created based on high-precision CT scan data, and the positions within the human body and connections to each other were carefully duplicated. The anatomical features of each internal organ were reflected in the modeling, and the material property data was defined referring to recent literature[11-21]. The biofidelity of the body region components were verified by comparing their impact responses with those in the literature data [22-25].

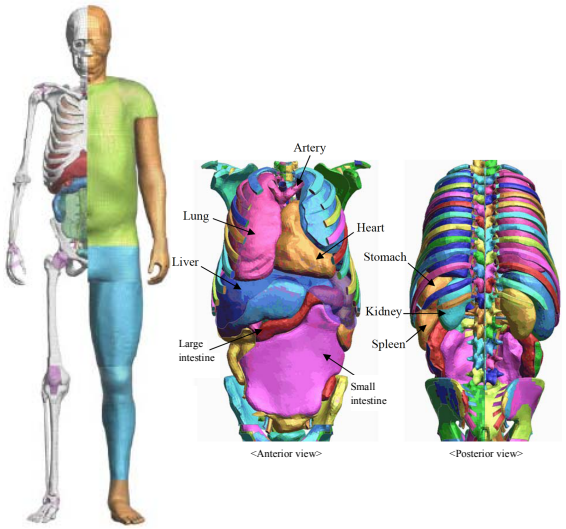

Figure 4. Outline of THUMS Version 4.

Validation of Body Region Component Models

This research assumed a condition in which a vehicle strikes a pedestrian from the side. The principal body region components that might sustain injuries are the head, chest, and knee. The mechanical response of these components against lateral impact was then verified.

<u>Impact Response of Head (Lateral Load)</u> - Figure 5 shows the model used by Yoganandan et al. (2004) to simulate a lateral impact test to the head [26]. In this test, the head was dropped with the side facing down so that it impacted on a pad set on top of a load cell at a speed of 3.5 to 6.0 m/s. This test was conducted on a total of ten PMHS and force response

corridors were then created for each impact speed. The force response corridors for the representative loading conditions (initial speed of 6.0 m/s) were then cited when verifying the force response of THUMS. Detailed descriptions of PMHS behavior immediately before the impact are not included in the literature, so it was assumed that the side of the head was perpendicular to the surface of the pad on impact. The force calculated at the surface of the load cell was then compared to the test results.

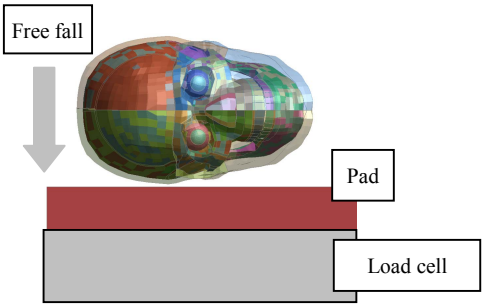

Figure 5. Lateral head impact test.

Figure 6 compares the time history curves of the forces measured and calculated at an impact speed of 6.0 m/s. The black lines are the test corridor and the red line is the force curve of THUMS. The results of THUMS are mostly within the test corridor. Figure 7 compares the peak force at impact speeds of 3.5, 4.9, and 6.0 m/s. The black line segments show the range of the force in the tests and the bar graphs show the peak force values of THUMS. The peak force values of THUMS are within the force ranges from the tests at all the impact speeds. With these comparison results, the research assumed that THUMS Version 4 closely simulated the impact response of the head against lateral impacts.

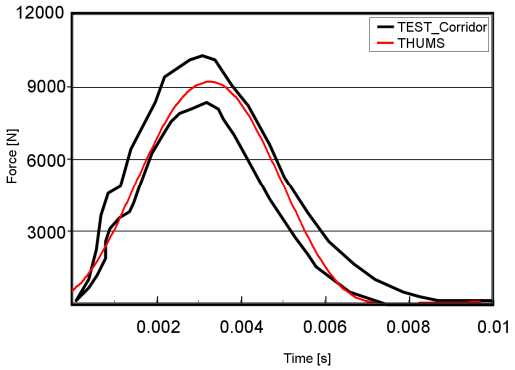

Figure 6. Force response curves of tests and THUMS (6.0 m/s).

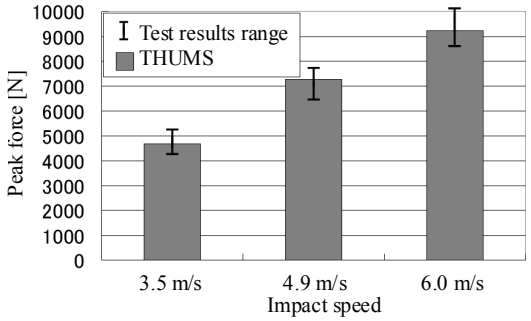

Figure 7. Peak force range of tests and THUMS.

<u>Impact Response of Chest (Lateral Load)</u> - Figure 8 shows a model simulating the lateral chest impact test performed by Viano et al. (1989) [27]. In this test, a cylindrically-shaped impactor with a mass of 23.4 kg is collided with the side of the chest of the PMHS at an initial speed of 3.6 to 10.2 m/s. The displacement of the impactor and the acceleration of the chest were measured during the test. This impact test was conducted on a total of 16 PMHS and force response corridors were created for each initial speed. The corridors for the representative loading conditions (initial speed of 4.5 m/s) were then cited when verifying the force responses of THUMS. The injuries sustained by each of the PMHS were described in the literature. The number of fractured ribs that occurred in a total of ten cases at initial speeds of 4.5 m/s and 6.5 m/s was referenced when verifying the results of THUMS. Detailed descriptions of the postures of the PMHS at the time of the tests are not included in the literature, so these postures were simulated based on the figures in the literature, and THUMS was arranged so that both arms were raised upwards. The impact force was calculated at the end of the impactor (the surface that makes contact with the side of the chest). The displacement of the impactor was obtained from the displacement of the nodes on the model and the deflection of the chest was found from the change in distance between the nodes on the surface of the side of the chest where the impact occurred, and the nodes on the opposite side of the chest from the impact.

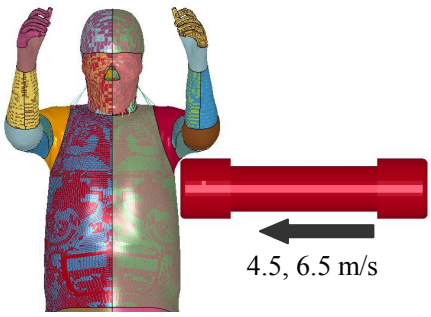

Figure 8. Lateral chest impact test.

Figure 9 compares the chest force response of the PMHS and THUMS with an initial speed of 4.5 m/s. The horizontal axis shows the chest deflection, and

the vertical axis shows the impact force. The force response of the PMHS is displayed by the grey corridor and the force response of the THUMS is shown by the red line. The upper limit of the test was a chest deflection of 50 mm at 3.2 kN, and the lower limit was a chest deflection of 60 mm at 1.5 kN. The result obtained from the THUMS was a chest deflection of 60 mm at 2.8 kN, so the result fell within the range of the upper and lower limits of the test.

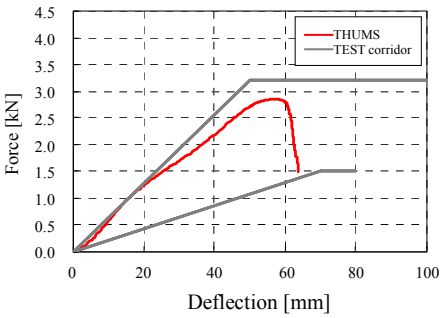

Figure 9. Comparison of chest load – chest deflection response.

Figure 10 compares the number of bone fractures in the ribs of the chest area in PMHS and THUMS. The vertical axis shows the number of rib fractures and the horizontal axis shows the initial speed. It was reported that, of the ten ribs in the PMHS used to verify THUMS in this research, eight were fractured in the tests performed by Viano et al[27]. The number of bone fractures ranged from 0 to 2 when the initial speed was 4.5 m/s, to a range of 2 to 7 fractures when the initial speed was 6.5 m/s. At 4.5 m/s, the number of fractured ribs with THUMS was 0, while at 6.5 m/s, the number of fractured ribs was 3. In both cases theses results were within the ranges established for the number of fractured bones in the tests. Furthermore, in this research it was assumed that a bone fracture occurred when the strain value calculated from the cortical bone shell elements exceeded 3%.
Based on the results described above, the research assumed that THUMS Version 4 closely simulated the impact response of the chest against lateral loading.

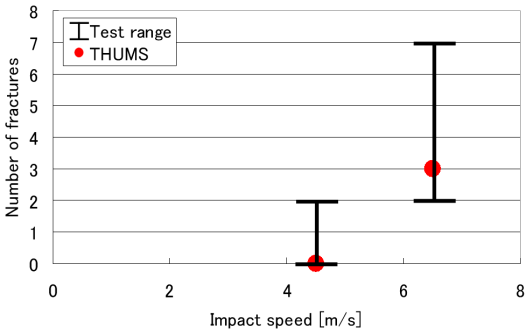

Figure 10. Number of rib fractures.

<u>Four-Point Bending Response of Knee</u> -
Figure 11 shows a model that simulates the knee joint bending test that was conducted by Bose et al. (2004) [28]. In this test, both ends of a PMHS knee (distal femur and proximal tibia) were fixed in place on a 4-point bending test device and the knee joint was moved and bent at an input velocity of 1.5 m/s. This test was conducted on a total of eight PMHS knee joints and a force response corridor was created. The force response corridor created from these PMHS tests was then compared to the FEM response. It was assumed that the ligaments in the knee ruptured when 16% elongation occurred.

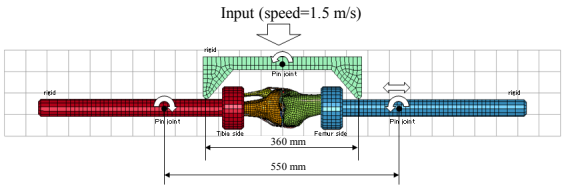

Figure 11. 4-point bending of knee joint.

Figure 12 compares the moment-bending angle corridor lines obtained from the test and the moment-bending angle line calculated using THUMS. The results obtained from THUMS (red line) indicate that up to a bending angle of 12.5 degrees the results stayed almost within the center of the test corridor (black dotted lines) and therefore were very consistent with the test results. It is estimated that when the bending angle of the knee joint in THUMS exceeded 12.5 degrees the ligaments ruptured. This is equivalent to a 40% risk of ligament rupture according to the results obtained from experimentation.
With these comparison results, the research assumed that THUMS Version 4 closely simulated the bending response of the knee joint in four-point bending.

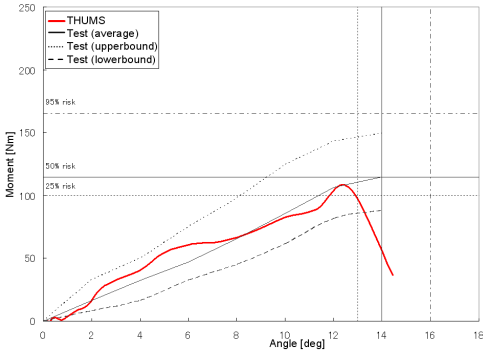

Figure 12. Relationship between moment and bending angle.

Verification of Pedestrian Behavior during Collision with SUV

Figure 13 shows a model that simulates a collision test between a PMHS and an SUV that was conducted by Schroeder et al. (2008) [3]. In this test, an SUV traveling at 40 km/h collided with a PMHS

that was being kept in a standing posture. Table 1 shows an outline of the test conditions. Scaling was performed on each portion of the body to make the physique of THUMS more closely match the proportions of the PMHS. The test conditions, such as the standing posture, were also simulated by referring to the descriptions in the literature. Figure 4 shows an outline of the PMHS and THUMS after it was modified. In this test, target markers were affixed to each portion of the PMHS and then the position of these markers was captured with a high speed camera to measure the trajectories during the collision. In the case of THUMS, the change in the node coordinates at each of the same positions as the target markers was outputted. In the test, the locations of the fractured ribs caused by the collision were recorded. Therefore, THUMS was used to predict rib fractures presuming that a fracture occurs when the strain of the cortical bones reached 3%.

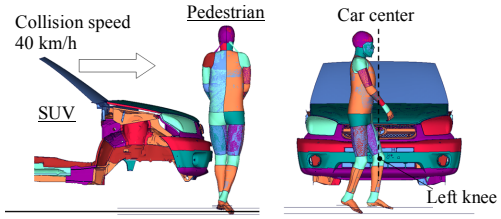

Figure 13. Simulation model of collision between pedestrian and SUV.

Table 1.
Pedestrian collision test conditions

	Test	THUMS
Vehicle type	SUV	SUV
Collision speed [km/h]	40	40
PMHS-height [cm]	185	185
Weight [kg]	85	84
Gender	Male	Male

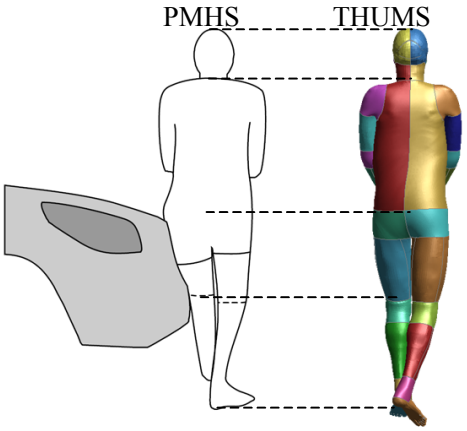

Figure 14. Pedestrian physique and posture .

Figure 15 shows the collision behavior of the PMHS from a posterior view, and Figure 16 shows the trajectories of each portion of the pedestrian's body according to the vehicle datum points. The gray lines in the figure are the trajectories of each portion obtained from the test and the red lines are the results calculated using THUMS. The full-body behavior of the pedestrian measured in the test and the results calculated using THUMS were mostly the same.

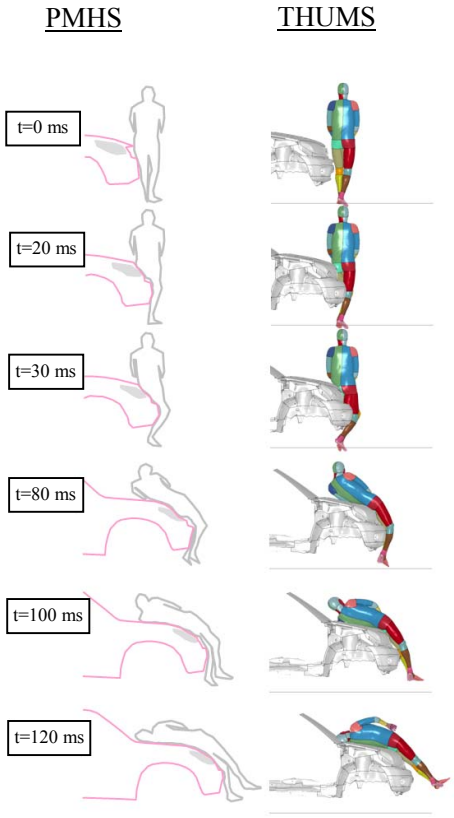

Figure 15. Pedestrian collision behavior .

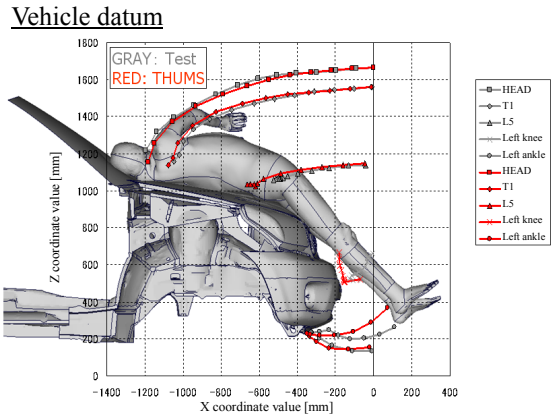

Figure 16. Comparison of pedestrian full-body behavior histories.

Figure 17 compares the PMHS autopsy results and the results predicted by THUMS for bone fractures in the chest region. From both the test and the THUMS simulation, two rib fractures were reported. However, a difference was seen in the locations where these fractures occurred. In the test, the injury was concentrated in the area where the pedestrian's arm was caught between the vehicle and the body, resulting in bone fractures (ribs #5 and #6). In the

case of THUMS, one rib was fractured in the same location (#6) and another rib fracture occurred where the vehicle hood and stomach collided (#10). This difference in the results was inferred to have resulted from differences in the shape of the skeleton in the PMHS and THUMS. The shape of the thorax in the THUMS model has large left and right dimensions in the lower region. It is conjectured that if the horizontal dimension of the inferior portion of the thorax cage of the PMHS is smaller, as shown in the diagram on the left side of Figure 17, then fractures of the lower ribs would not be as likely to occur. Further research is necessary to look into the relationship between the shape of the thorax cage and rib fractures.

PMHS THUMS

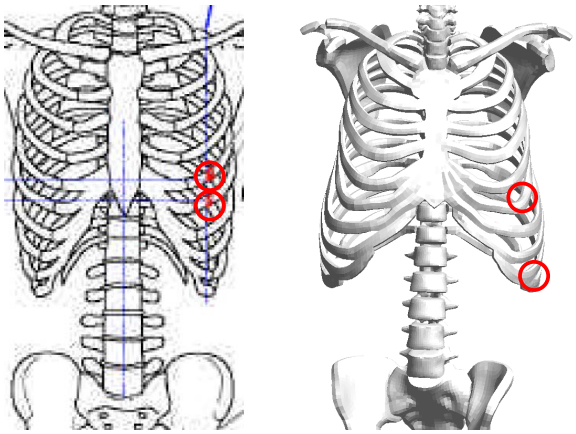

Figure 17. Comparison of rib fracture locations.

Figure 18 compares the locations of ligament ruptures in the knee. In both the test and THUMS, the ACL, PCL, and MCL were all ruptured on the side of the collision (left leg). Furthermore, the areas in the knee where these ligament ruptures occurred were very consistent in both the test and in THUMS. Consequently, after using THUMS Version 4 to predict pedestrian behavior and injuries in the event of a collision with an SUV, the results indicated that THUMS was able to largely reproduce the same results as in tests using PMHS. Therefore, the research assumed that THUMS Version 4 is capable of investigating the dependency of pedestrian injuries on the collision speed.

PMHS THUMS

ACL: detached ACL: detached

PCL: detached PCL: ruptured

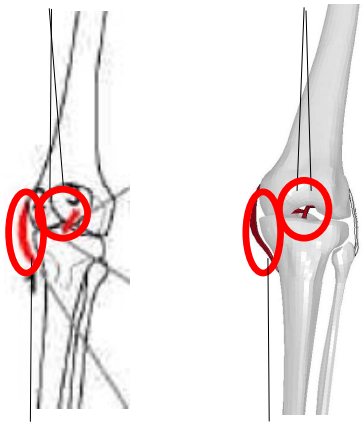

MCL: ruptured MCL: ruptured

Figure 18. Comparison of ligament rupture conditions.

METHODOLOGY

The validated THUMS Version 4 was used to analyze collisions between an SUV and a pedestrian at different collision speeds. Table 2 shows the colliding conditions.

Injury reference criteria values were defined for each body region referring to the literature (Table 3).

For estimating head injuries, the head injury criterion (HIC) and the principal strain on the brain (white matter) were evaluated [29-30]. It was assumed that a skull fracture would occur if the HIC value was 700 or higher. It was also assumed that brain tissue damage and cerebral contusion would occur when the principal strain on the brain white matter exceeded 30%.

For estimating chest injuries, the research monitored rib fractures and the human body tolerance thresholds of the principal internal organs [31-32]. It was assumed that a heart laceration would occur when the principal strain exceeded 30%, while a liver laceration would occur when the strain was 40% or higher.

Table 2.
Colliding conditions

	A	B	C	D	E	F
Collision speed [km/h]	20	30	40	50	60	65

Table 3.
Assumed threshold values

Region	Evaluation index	Reference criteria values
Head (skull)	HIC	700 or more
Brain	Principal strain	30% or higher
Rib (cortical bone)	Plastic strain	3% or higher
Heart	Principal strain	30% or higher
Liver	Principal strain	40% or higher

RESULTS

Of the analysis results obtained under all six colliding conditions (20 to 65 km/h), a significant difference in the injury prediction results was found in the three cases where the collision speed was 30, 40, and 50 km/h (Table 4). This paper compares the full-body behavior and occurrence of injury with an emphasis on these three conditions.

Table 4.
Injury prediction results

Region	Injury	Collision speed					
		20	30	40	50	60	65
Head	Skull fracture	-	-	-	-	-	-
	Cerebral contusion	-	-	Occurred	Occurred	Occurred	Occurred
Chest	Rib fracture	-	-	Occurred	Occurred	Occurred	Occurred
	Heart damage	-	-	-	Occurred	Occurred	Occurred
	Liver damage	-	-	-	-	-	-

Full-Body Behavior

Figures 19 to 21 show the pedestrian behavior during the collisions. At a collision speed of 30 km/h, the knee and vehicle bumper make contact first, and then the hip, side of the stomach, and chest (shoulder) collide with the hood of the vehicle in that order. Finally, the head collides with the windshield glass. When the collision speed is 40 km/h or more, the collision from the knee to the hip with the vehicle is the same as at 30 km/h. However, the chest (shoulder) collides with the cowl portion at the back end of the hood. The head collides with the windshield in the same way as it does at a collision speed of 30 km/h.

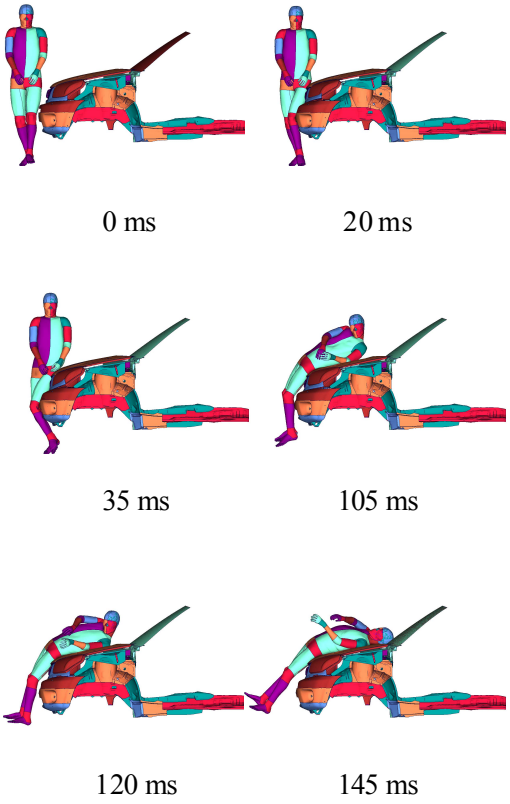

Figure 19. Pedestrian behavior at collision speed of 30 km/h.

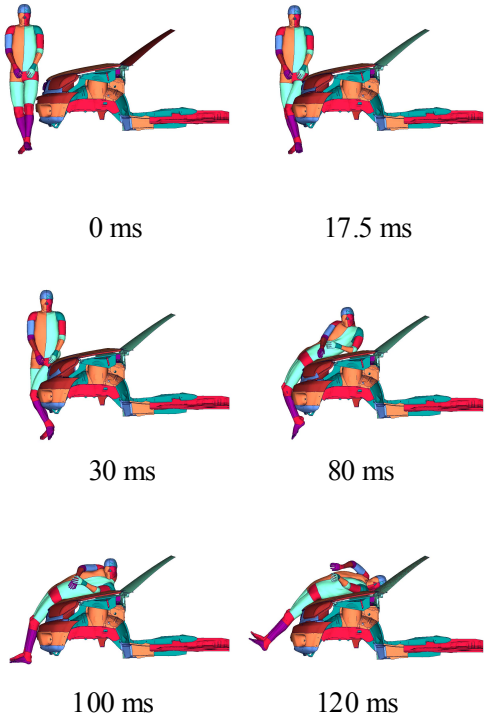

Figure 20. Pedestrian behavior at collision speed of 40 km/h.

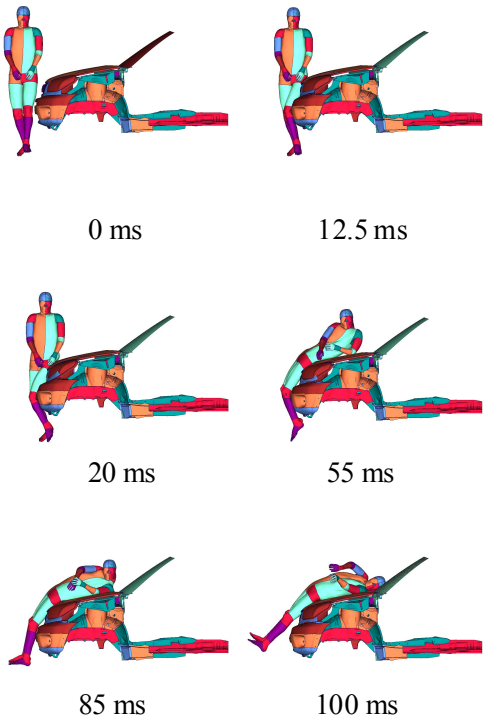

Figure 21. Pedestrian behavior at collision speed of 50 km/h.

Contact Reaction Force during Collision

Figure 22 shows the time history curves of the contact reaction force that the pedestrian receives from the vehicle. The force rises when the bumper collides with the knee and a substantial increase occurs when the hip collides with the edge of the hood. After this, the force reaches its first peak when the side of the stomach collides with the hood and the third force peak appears when the shoulder collides with the hood. The peaks of these forces increase in accordance with the increase in the collision speed.

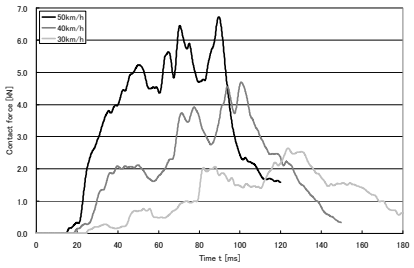

Figure 22. Contact reaction force of pedestrian and vehicle at different collision speeds.

Head Injuries

Table 5 shows the HIC values calculated at each collision speed. All the HIC values were less than the reference criterion value of 700, at which injuries occur, and were generally low values. Figure 23 shows contour maps of the principal strain observed in a central cross section of the brain. It was estimated that at a collision speed of 40 km/h or higher, principal strain exceeded 30%, which is assumed to be the reference criterion value of brain injury.

Table 5.
Head impact responses

		20 km/h	30 km/h	40 km/h	50 km/h	60 km/h	65 km/h
Head	HIC	271	39	214	280	512	512
	Angular velocity [rad/s]	104	64.8	90.7	99.7	207.6	208.5
	Angular acceleration [rad/s^2]	4484	6840	12300	12000	13080	13283

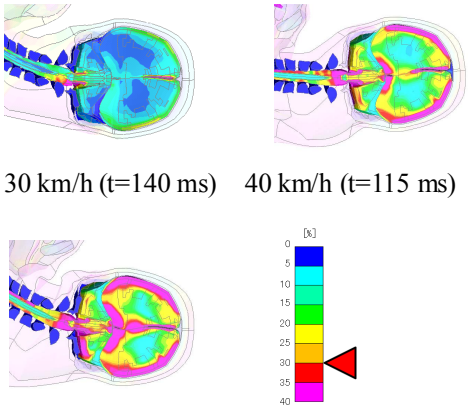

Figure 23. Contour map of principal strain in brain.

Chest Injuries

Table 6 shows the locations on the vehicle hood where the chest collided, the number of fractured ribs, and the compression rate of the chest. Furthermore, Figure 24 shows the locations of fractured ribs depending on the collision speed. At a collision speed of 30 km/h there were no fractured ribs, but at a collision speed of 40 km/h, two ribs were fractured on the side of the body that collided with the hood of the vehicle. At a collision speed of 50 km/h a total of seven ribs were fractured, including ribs on the opposite side of the body from the collision.

Table 6.
Chest impact responses

		20 km/h	30 km/h	40 km/h	50 km/h	60 km/h	65 km/h
Chest	Location of shoulder impact	Hood	Hood	Cowl	Cowl	Cowl – windshield-glass	Cowl – windshield-glass
	Bone fractures	None	None	2	7	14	12
	Chest compression rate (Cmax)	15	16.1	20.1	30.2	42.3	40.5

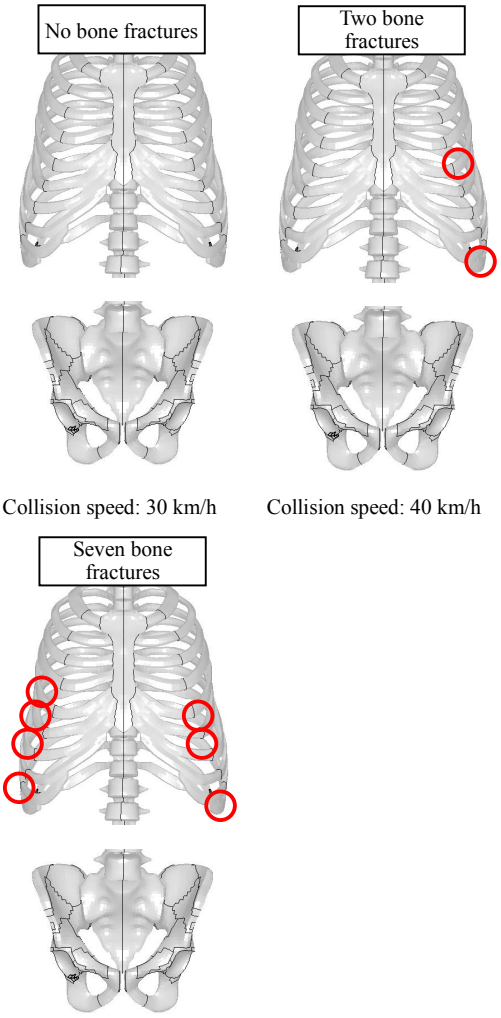

Figure 24. Locations of rib fractures.

Figures 25 and 26 show contour maps of the principal strain observed in a central cross section of the heart and liver. The calculated strain in the heart exceeded 30% at a collision speed of 40 km/h, while the area in which strain exceeded 30% expanded to cover the entire area of the heart at a collision speed of 50 km/h. On the other hand, the range of principal strain that exceeded 40% in the liver at a collision speed of 50 km/h was localized (an area of less than 3% of the total area of the liver).

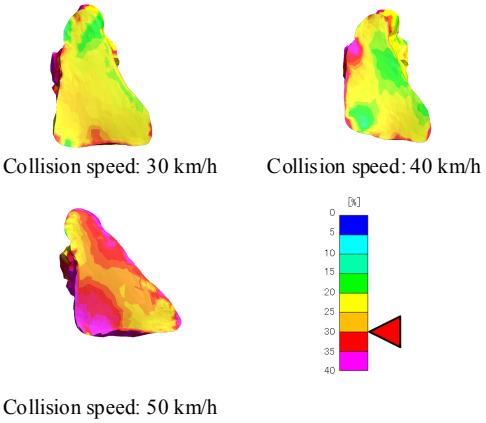

Figure 25. Contour map of principal strain in heart.

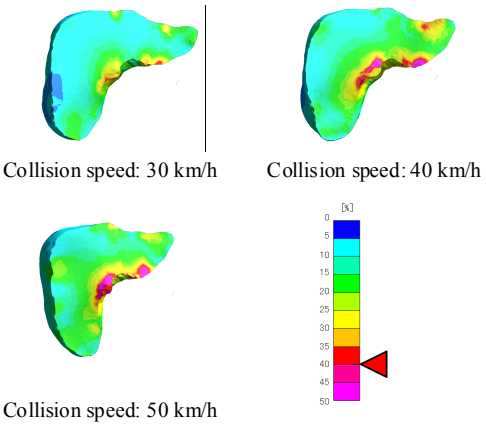

Figure 26. Contour map of principal strain in liver.

DISCUSSION

Relationship between Collision Speed and Brain Injury

The risk of incurring the serious DAI brain injury has been proposed by Margulies et al. (1992) [32]. Figure 27 shows the relationship between the risk of DAI and the angular velocity and angular acceleration of the head. Margulies et al. proposed that the risk of DAI increases when the angular acceleration of the head is 8,000 rad/s^2 or more, or the change in the angular velocity of the head is in the range of 80 rad/s or more (area A in Figure 27). The results of the investigation under the three conditions (collision speeds of 30, 40, and 50 km/h) were inserted into this figure. It was found that the results fell outside at a collision speed of 30 km/h, but that the results fell within area A at collision speeds of 40 km/h or more. Therefore, there is a high risk of DAI occurring at these speeds.

For reference, an evaluation using the cumulative strain damage measure (CSDM) proposed by Thakhounts et al. (2003) [33] was also performed. CSDM is an evaluation index for the occurrence of DAI that uses the amount of strain placed on the

brain. It assumes that DAI occurs when a principal strain that exceeds 25% is present in an area that exceeds 54% of the entire brain area. Figure 28 shows the relationship between the collision speed and CSDM. As shown in Figure 23, when the distribution of principal strain in the brain at a collision speed of 40 km/h or more is considered, the scope of the area where the principal strain exceeds 25% expands significantly. The CSDM (0.25) values also confirm a major increase (35%) between collision speeds of 30 and 40 km/h. CSDM exceeds 54%, which is said to be the criterion value at which brain injuries occur, at a collision speed of 40 km/h or more.

Based on the results described above, the results of the evaluations using angular acceleration and strain-based CSDM at three collision speeds showed that the risk of receiving a brain or other head injury increased when the collision speed was 40 km/h or more.

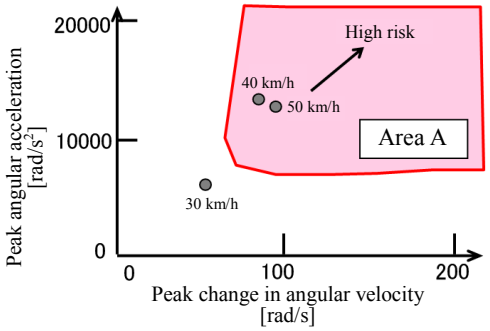

Figure 27. Relationship between angular velocity and angular acceleration of head and DAI risk.

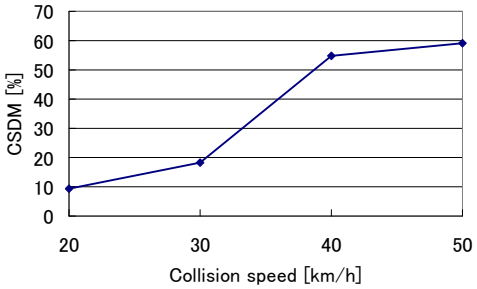

Figure 28. Relationship between collision speed and CSDM.

Mechanism Linking Angular Velocity of Head to Increase in Brain Strain

This research investigated a collision between an SUV and a pedestrian. When the collision speed exceeded 40 km/h, the shoulder of the pedestrian collided with the hard cowl portion located at the rear end of the vehicle's hood and the movement of the chest was greatly decelerated, which produced a large difference in the velocities of the head and the chest (Figure 29). As a result, the angular velocity of the head increased greatly. Furthermore, it is thought that when the translational movement of the head changes into angular motion, a tensile force is generated near to the spinal cord (Figure 30). It is presumed that this increase in the angular velocity of the head and the tensile force generated near to the spinal cord are the causes of the principal strain that is generated near the surface of the brain and near the spinal cord (Figure 31). Therefore, it can be inferred that if the impact of the collision between the shoulder and the hood is lessened, then it may be possible to reduce the angular velocity of the head. In addition, because the head collided with the windshield glass under the conditions in this investigation, the strain on the head due to direct impact was small and the HIC values were also all less than 700.

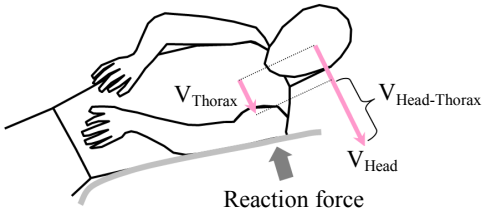

Figure 29. Head and chest velocity pattern diagram at time of shoulder impact.

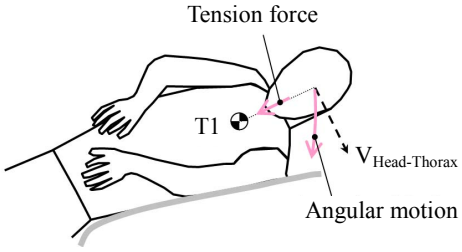

Figure 30. Generation of tensile force and angular motion of head due to difference in velocity between head and chest.

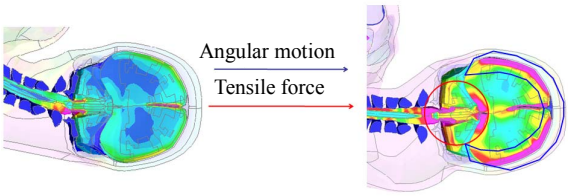

30 km/h 40 km/h

Figure 31. Principal strain generated in brain due to angular motion and tensile force.

Relationship between Collision Speed and Internal Organ Injuries

As shown in Figure 22, when the collision speed of the vehicle increases, the force that acts on the chest of the pedestrian also increases greatly. At a collision speed of 50 km/h the collision force on the side of the stomach is approximately 5 kN and rib fractures occur on both sides of the body. Deformation of the

thorax increases due to this expansion of the area where rib fractures occur and it is assumed that this leads to an increase in the force on the internal organs. Figure 32 shows the amount of deformation of the thorax depending on the collision speed, while Figure 33 shows the human body tolerance threshold excess ratio of the heart (principal strain is 30% or more) depending on the collision speed. It was found that at a collision speed of 50 km/h, there was a significant increase in the deformation of the thorax and also an expansion of the scope of the strain that was generated on the heart.
Based on the fact that serious brain injuries are predicted to occur when the collision speed is 40 km/h or more and that heart damage is predicted to occur when the collision speed is 50 km/h or more, it was inferred that the fatality risk for pedestrians involved in a collision with a vehicle increases when the collision speed is 40 km/h or more.

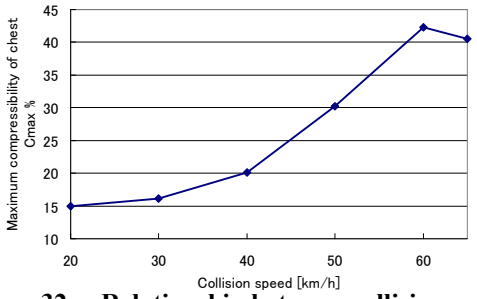

Figure 32. Relationship between collision speed and thorax deformation ratio.

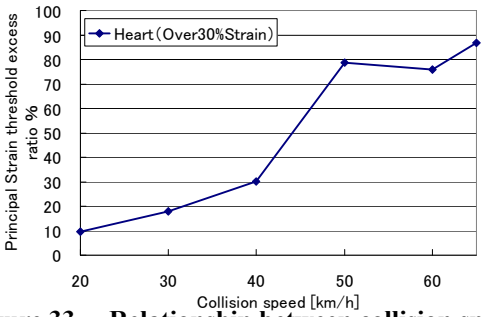

Figure 33. Relationship between collision speed and heart strain.

Limitations

In the calculations conducted in this research it was assumed that an SUV impacts a pedestrian from the side and that the collision is centered in the middle of the vehicle's front end. In an actual accident the pedestrian's physique and posture at the time of the collision, and the shape of the vehicle will all likely vary greatly from these conditions. The results of this research are not intended to explain all accidents involving pedestrians. Furthermore, this research used what was considered to be mean values for the human body tolerance thresholds, which were determined after consulting a wide variety of literature on the topic, in consideration of the great differences that exist among individuals. In the future more research that takes these differences among individuals into account, such as the decrease in the tolerance thresholds due to aging, will be necessary.

CONCLUSION

1. The THUMS Version 4 pedestrian model was used to simulate a collision between a pedestrian and an SUV as described in the literature. It was estimated that THUMS Version 4 successfully simulates the full-body behavior of the pedestrian (PMHS) reported in the literature.

2. Using the validated THUMS Version 4 pedestrian model, the research investigated the relationship of pedestrian head and chest injuries with collision speed.
- It was predicted that the risk of head and chest injuries is lower up to a collision speed of 30 km/h, but that this risk increases at collision speeds of 40 km/h or more.
- When the collision speed exceeds 40 km/h, the pedestrian shoulder collided with the back end of the vehicle's hood and the translational movement of the chest was stopped violently. As a result, the angular acceleration of the head increased greatly and the risk of DAI also increased.
- Moreover, at collision speeds of 50 km/h or more, rib fractures were predicted on both the left and right sides of the body, the deformation of the thorax increased greatly and the risk of sustaining a heart injury was also higher.
The research findings described above were consistent with the trends cited in accident data that the fatality risk for pedestrians increases when the collision speed is 40 km/h or more.

ACKNOWLEDGMENTS

The authors would like to thank Toyota Technical Development Corporation for its assistance with the modeling and simulation work.

REFERENCES

[1] Traffic accident statistics annual report. 2009. Institute for Traffic Accident Research and Data Analysis.

[2] R. W. G. Anderson, A. J. McLean, M. J. B. Farmer, and B. H. Lee. 1995. "Vehicle Travel Speeds and the Incidence of Fatal Pedestrian Crashes." International Research Council on the Biomechanics of Impacts (IRCOBI), 107-117.

[3] G. Schroeder, K. Fukuyama, K. Yamazaki, K. Kamiji, and T. Yasuki. 2008. "Injury Mechanism of Pedestrians Impact test with a Sport-utility Vehicle and Mini-van." IRCOBI, 259-273.

[4] D. Subit, J. Kerrigan, J. Crandall, K. Fukuyama, K. Yamazaki, K. Kamiji, and T. Yasuki. 2008. “Pedestrian-Vehicle Interaction: Kinematics and Injury Analysis of Four Full-Scale Tests.” IRCOBI, 275-294.

[5] J. Kerrigan, D. Subit, C. Untaroiu, and J. Crandall. 2008. “Pedestrian Lower Extremity Response and Injury: A Small Sedan vs A Large Sport Utility Vehicle.” SAE, SAE2008-01-1245.

[6] J. Kerrigan, C. Kam, C. Drinkwater, D. Murphy, D. Bose, J. Ivarsson, and J. Crandall. 2005. “Kinematic Comparison of the POLAR- and PMHS in Pedestrian Impact Test with a Sport-Utility Vehicle.” IRCOBI, 159-174.

[7] T. Yasuki. 2005. “A Survey on the Biofidelity of the Knee Bending Angle of the TRL Lower Leg Impactor.” 19thESV, 05-0101.

[8] H. Miyazaki, F. Matsuoka, M. Kuwahara, Y. Kitagawa, and T. Yasuki. 2009. “Development of Flexible Pedestrian Legform Impactor FE model and Comparative study with Leg Behavior of Human FE Model THUMS.” 21st ESV, 09-0112.

[9] A. Tamura, Y. Nakahira, M. Iwamoto, I. Watanabe., K. Miki, S. Hayashi, and T. Yasuki. 2006. “The Influence of the Traction Force Due to Inertia of the Brain Mass on Traumatic Brain Injury during SUV-to-Pedestrian Impact.” IRCOBI.

[10] THUMS Users Manual. (2010).

[11] J. A. W. van Dommelen, B. J. Ivarsson, M. M. Jolandan, S. A. Millington, M. Raut, J. R. Kerrigan, J. R. Crandall, and D. R. Diduch. 2005. “Characterization of Rate-Dependent Mechanical Properties and Failure of Human Knee Ligaments.” SAE, SAE2005-01-0293.

[12] H. Yamada. 1970. “Strength of Biological Materials.” F. G. Evean, Ed., The Williams & Wilkins Company, Baltimore.

[13] H. Abe, K. Hayashi, and M. Sato. 1996. “Data Book on Mechanical Properties of Living Cells, Tissues and Organs.” Springer-Verlag. Tokyo.

[14] C. S. Shah, K. H. Yang, W. Hardy, H. K. Wang, and A. I. King. 2001. “Development of a Computer Model to Predict Aortic Rupture due to Impact Loading.” Stapp Car Crash Journal, Vol. 45, 161-182.

[15] J. B. Lee and K. H. Yang. 2001. “Development of a Finite Element Model of the Human Abdomen.” Stapp Car Crash Journal, Vol. 45, 79-100.

[16] D. Cesari and R. Bouquet. 1990. “Behaviour of Human Surrogates Thorax under Belt Loading.” SAE902310.

[17] J. Cavanaugh, G. Nyquist, S. Goldberg, and A. King. 1986. “Lower Abdominal Tolerance and Response.” SAE861978.

[18] C. Foster, W. Hardy, K. Yang, A. King, and S. Hashimoto. 2006. “High-Speed Seatbelt Pretensioner Loading of the Abdomen.” Stapp Car Crash Journal, Vol. 50, 27-51.

[19] A. Kemper, S. Duma, F. Matsuoka, and M. Masuda. 2005. “Biofidelity of the SID-ＩＩs and a Modified SID-IIs Upper Extremity: Biomechanical Properties of the Human Humerus.” Proc. 19th ESV Conference, 05-0123.

[20] A. Kemper, C. McNally, E. Kennedy, A. Rath, S. Manoogian, J. Stitzel, and S. Duma. 2005. “Material Properties of Human Rib Cortical Bone from Dynamic Tension Coupon Testing.” Stapp Car Crash Journal, Vol. 49, 199-230.

[21] E. S. Karl, P. M. Wilbur, C. C. Chales, and A. L. Averill. 1958. “Mechanisms in Development of Interstitial Emphysema and Air Embolism on Decompression from Depth.” Journal of Applied Physiology, Vol. 13, 15-29.

[22] R. W. Nightingale, J. H. McElhaney, D. L. Camacho, M. Kleinbberger, B. A. Winkelstein, and B. S. Myers. 1997. “The Dynamic Responses of the Cervical Spine: Buckling, End Conditions, and Tolerance in Compressive Impacts.” Proceedings of 42nd Stapp Car Crash Conference.

[23] C. K. Kroell, D. C. Schneider, and A. M. Nahum. 1971. “Impact Tolerance and Response of the Human Thorax.” Proc. 15th Stapp Car Crash Conference, 84-134.

[24] C. K. Kroell, D. C. Schneider, and A. M. Nahum. 1971. “Impact Tolerance and Response of the Human Thorax II.” Proc. 18th Stapp Car Crash Conference, 383-457.

[25] K. Shigeta, Y. Kitagawa, and T. Yasuki. 2009. “Development of Next Generation Human FE Model Capable of Organ Injury Prediction.” 21st ESV, 09-0111.

[26] N. Yoganandan, J. Zhang, and F. A. Pintar. 2004 “Force and Acceleration Corridors from Lateral Head Impact.” Traffic Injury Prevention, 368-373.

[27] D. C. Viano. 1989. “Biomechanical Responses and Injuries in Blunt Lateral Impact.” 33rd Stapp Car Crash Conference, SAE892432.

[28] D. Bose, K. Bhalla, L. Rooji, S. Millington, A. Studley, and J. Crandall. 2004. “Response of the Knee Joint to the Pedestrian Impact Loading Environment.” SAE2004-01-1608.

[29] J. M. Abel, T. A. Gennarelli, and H. Segawa. 1978. “Incidence and Severity of Cerebral Concussion in the Rhesus Monkey Following Sagittal Plane Angular Acceleration.” STAPP, 780886.

[30] S. S. Margulies, L. E. Thibault, and T. A. Gennarelli. 1985. “A Study of Scaling and Head Injury Criteria Using Physical Model Experiments.” IRCOBI, SAE1985-13-0015.

[31] J. W. Melvin, R. L. Stalnaker, and V. L. Roberts. 1973. “Impact Injury Mechanisms in Abdominal Organs.” 17th Stapp Car Crash Conference, SAE730968.

[32] S. S. Margulies and L. E. Thibault. 1992. “A Proposed Tolerance Criterion for Diffuse Axonal Injury in Man.” Journal of Biomechanics, Vol. 25 No. 8 917-923.

[33] E. G. Thakhounts. 2003. “On the Development of the SIMon Finite Element Head Model.” Stapp Car Crash Journal, Vol. 47.